Author Manuscript

Author Manuscript

Author Manuscript

Author Manuscript

HHS Public Access

Author manuscript

Lab Chip. Author manuscript; available in PMC 2015 March 17.

Published in final edited form as:

Lab Chip. 2014 January 21; 14(2): 302–314. doi:10.1039/c3lc51052b.

Microfluidic transwell inserts for generation of tissue culture-friendly gradients in well plates

Christopher G. Sip, **Nirveek Bhattacharjee**, and **Albert Folch**

Abstract

Gradients of biochemical molecules play a key role in many physiological processes such as axon growth, tissue morphogenesis, and trans-epithelium nutrient transport, as well as in pathophysiological phenomena such as wound healing, immune response, bacterial invasion, and cancer metastasis. In this paper, we report a microfluidic transwell insert for generating quantifiable concentration gradients in a user-friendly and modular format that is compatible with conventional cell cultures and with tissue explant cultures. The device is simply inserted into a standard 6-well plate, where it hangs self-supported at a distance of ~250 μm above the cell culture surface. The gradient is created by small microflows from the device, through an integrated track-etched porous membrane, into the cell culture well. The microfluidic transwell can deliver stable, quantifiable gradients over a large area with extremely low fluid shear stress to dissociated cells or tissue explants cultured independently on the surface of a 6-well plate. We used finite-element modeling to describe the porous membrane flow and molecular transport and to predict gradients generated by the device. Using the device, we applied a gradient of the chemotactic peptide N-Formyl-Met-Leu-Phe (fMLP) to a large population of HL-60 cells (a neutrophil cell line) and directly observed the migration with time-lapse microscopy. On quantification of the chemotactic response with an automated tracking algorithm, we found 74% of the cells moving towards the gradient. Additionally, the modular design and low fluid shear stress made it possible to apply gradients of growth factors and second messengers to mouse retinal explant cultures. With a simplified interface and well-defined gradients, the microfluidic transwell device has potential for broad applications to gradient-sensing biology.

Introduction

The sensing of chemical gradients plays an important role in the guidance of cells for tissue development[1], migration of cells in the immune system[2], and human disease[3]. Gradients of morphogens guide the development of tissue and organ structure[4], chemokines recruit leukocytes and lymphocytes during the inflammatory response[5,2], and guidance factors direct axon path finding in the developing nervous system[6–8]. Pathological gradient sensing mechanisms are involved in cancer metastasis[9], autoimmune diseases[10], infections, implant rejection, and chronic inflammatory diseases[11]. Modeling of receptor-ligand interactions, molecular transport, and cellular mechanisms has elucidated many of the processes involved in gradient sensing[12,4,13]. Continued efforts to further our understanding of gradient biology are important to the development of drugs and therapeutic interventions. For example, stem cells naturally migrate to the site of injury for regenerative stem cell therapy[14–17], and engineered T-cells are designed to target cancer for adoptive immunotherapy[18].

Author Manuscript Author Manuscript Author Manuscript Author Manuscript

With the broad relevance of gradient sensing in biology, manipulation of the cell microenvironment is a critical technique for in vitro research. Conventional in vitro technique has relied primarily on four types of assays to apply concentration gradients to cell and tissue cultures: porous membranes[19], micropipette assays[20], chamber assays[21,22], and gel assays[23,24]. Across these assays, there is a compromise between the number of cells, length of gradients, quality of imaging, and ease-of-use. These limitations and the desire to control the timing and shape of gradients, have motivated development of new assays based on microfluidic technology[25].

Microfluidic laminar flow makes possible the generation of stable, quantifiable, and reproducible gradients[25–27]. A variety of mixing schemes have been explored to produce gradients having arbitrary shapes in space and/or time[28–31]. Flow-based gradient devices have been used to study a range of gradient sensing biology including chemotaxis[32,33], differentiation[34], and cancer cell migration[35]; however fluid shear stress exerted on cells has been a major limitation[36].

Others have demonstrated control of gradients using diffusion of solutes in flow-free conditions[25–27]. In these designs, flows through adjacent microchannels are used to intermittently exchange solutions for short-term gradients[37,38] or maintain steady state[39–42]. Since gradient generation is based on diffusive mixing, flow-free devices are generally simpler to operate, negate harmful shear flow, and many are pipette-accessible. However, slow time scales for gradient evolution limit the dynamic control of gradients, and the visualization of cells in gels is less than optimal.

More recently, several devices have been demonstrated in which integrated porous membranes deliver gradients to cell cultures while isolating microchannel flows[43–50]. Typically, thin porous filter membranes are used because they can be integrated directly between layers of micromolded PDMS. In these types of devices, cells have been cultured on a surface opposite the membrane[43,46,47,49] or directly on the membrane[44,48,50]. Culture opposite the membrane has the advantage of improved optical clarity because the pores of the membrane are out of focus, whereas cells cultured directly on the membrane further restrict flow through the pores. Across reported devices, there exist a range of fabrication strategies for integrating the porous membrane due to challenges with bonding PDMS and the porous membranes. Additionally, there are various opinions regarding the ability to neglect flow through the membrane and consider only diffusive transport (for contrasting opinions compare Morel et al.[49] and VanDersal et al.[47] with Kim et al.[50] and Kawada et al.[48]). Regardless, porous membranes are a promising approach to interfacing microfluidics with cell cultures; however, future progress will benefit from efforts to simplify device operation and characterize membrane flows.

In this paper, we describe a new microfluidic chemotaxis assay that was designed to satisfy the following five criteria to promote wider adoption in non-microfluidic laboratories: (1) A quantitative measure of the gradients must be obtainable during live-cell assays. (2) The device must allow for assaying large numbers of cells or large tissue area. (3) Cells must be directly observed under the microscope while in the device. (4) Operation of the device must be user-friendly by the standards of biologists. (5) Setup, operation or imaging of the

Author Manuscript Author Manuscript Author Manuscript Author Manuscript

gradient must be compatible with conventional cell culture techniques and surface micropatterning technologies[51] to permit the study of combinatorial gradient sensing with cell-surface, cell-cell, and long-range guidance factors[6].

Current microfluidic approaches generally do not provide simple methods for interfacing with cell cultures. In typical designs, cells are injected into microchannels therefore conventional protocols for cell culture and substrate preparation must be adapted. For sensitive cell culture types such as primary neurons, long-term culture within microchannels can be challenging due to shear sensitivity. To address these issues we have developed a novel microfluidic 'microfluidic transwell insert' that interfaces with standardized 6-well plate cell cultures. With this design, we demonstrate generation of large-area steady-state gradients that exert extremely low fluid shear stress. These characteristics make the technology well suited for a variety of sensitive cell cultures and enable application to tissue explants that are impractical to culture within microchannels.

In this paper we describe the methods for fabrication of devices, theory and finite-element modeling (FEM) for predicting flows, and characterization of devices using fluorescence microscopy. We also demonstrate application of the microfluidic transwell insert for observing chemotaxis of neutrophil-like cells and applying gradients to mouse embryonic retinal explants.

Materials and methods

Microfluidic transwell insert design

The goal of this work was to develop a user-friendly microfluidic concentration gradient generator that can be used with conventional cell culture technique. Our approach is based on controlling fluid delivery between the device and cell culture through high resistance track-etched membranes. The track-etched membrane serves to compartmentalize flows and enable modular application of the device to standard 6-well plates. The microfluidic transwell insert is designed for generating large-area gradients and straightforward application to cells cultured independently of the device and using conventional technique.

The microfluidic transwell insert has several key design aspects: (1) the insert device is applied by simply placing it into the well of a 6-well plate where it is self-supported at a short distance (approximately 250 μm) above the cell culture surface. The device is untethered from the substrate; therefore, timing and orientation of the gradient is controlled by its physical application to the well. (2) Solutions are delivered to the well through areas of a high-resistance track-etched membrane via microchannels to generate gradients across and above the cell culture surface. (3) Flow within the device maintains an unlimited source and sink for soluble factors and long-term, stable gradient generation. (4) Cells or tissue explants can be cultured on standard glass-bottom 6-well plates independent of the device. (5) The device materials, PDMS and polyethylene terephthalate (PET), are transparent which permits real-time observations of cell morphology and migration during the course of the gradient application. (6) The track-etched PET membrane shields cells from exposure to shear flows because of its high fluidic resistance.

Author Manuscript Author Manuscript Author Manuscript Author Manuscript

The 3D renderings in Fig. 1(A–B) depict the microfluidic transwell insert and the application of a device to a standard glass-bottom 6-well plate. Cross-sectional schematics in Fig. 1(C–E) show the orientation of the device when inserted in a standard glass-bottom 6-well and generation of a concentration gradient. The untethered design and the modular interface simplify integration with existing cell culture and protocols. The photographs in Fig. 1(F–G) show the device filled with dye solutions to visualize the microchannel architecture and gradient. Further details about the design of hydraulic resistances and permeability of the membrane are described in Supplemental Document A.

Multilayer soft lithography

Fabrication of transwell microfluidic inserts was accomplished using multilayer soft-lithography of PDMS replicas, oxygen plasma for PDMS-PDMS bonding, and silane coupling for PDMS bonding to membranes. The device was assembled from 4 parts including an injection-molded plastic support, embedded PDMS replica, a thin PDMS layer, and a track-etched membrane (Fig. 2). For fabrication of master molds, silicon wafers were spin-coated with SU-8 2000 series photoresists (Microchem Co., Newton, MA) and photopatterned using multilayer photolithography. For the master mold to the embedded layer shown in Fig. 2(B), a 75 μm thick layer was spin-coated using SU-8 2075 at 3000 rpm to define the inlet and outlet channels. After post-exposure baking of the first layer, a second layer of 100 μm was spin-coated using SU-8 2075 at 2125 rpm to pattern the low-resistance channel that feeds flow to the membrane and to a common outlet. The master of the thin PDMS replica layer (Fig. 2(C)) was designed to produce a perforated PDMS layer through exclusion-molding technique. The features for the molding of the gradient delivery channels were patterned with a 200 μm thick layer of SU-8 (produced by spin-coating SU-8 2075 at 2125 rpm and pre-baking twice). Next, an additional 200 μm thick layer was spin-coated to pattern the vias and boundary features. After photopatterning, post-exposure baking, and development of the SU-8, masters were hard baked at 150 °C on a hotplate. Masters were then treated using several drops of a fluorinated-trichlorosilane (#448931, Sigma, St. Louis, MO) in a desiccator under house vacuum.

Embedding of PDMS into plastic supports

The top microchannel layer of the microfluidic transwell insert was replica molded to embed the PDMS into a plastic support (see Fig. S1(a) in supplemental information). The plastic supports from Transwell-brand inserts were harvested by removing the track-etched membrane. The supports were oxygen plasma treated, then the inside surface is coated with a 1% APTES, 1% vinyl silane, 5% water, 93% methanol solution using a cotton swab and allowed to air dry in a chemical fume hood. We found that without the vinyl/APTES silane treatment, PDMS of the embedded layer cured within the plastic support could be easily detached under mild force such as punching holes for inlets. Spacers of 34 mm outer diameter and 18 mm inner diameter were made by laser cutting a stack consisting of a .06″ thick acrylic sheet and an adhesive backed 10 mil thick acrylic film. Spacers were fixed onto the SU-8 photopatterned master to provide a pedestal for the plastic support during molding. As a result of the spacer, the featured surface of the embedded PDMS extends past the plastic support and nests into the 20 mm diameter miniature well of the cover-glass bottom 6-well (Fig. S1(b)). The silane-modified supports were lightly dipped in uncured PDMS,

Author Manuscript Author Manuscript Author Manuscript Author Manuscript

placed on the spacers, and baked at 80 °C on a hotplate to secure in place on the master mold. After curing and cooling to room temperature, uncured PDMS (mixed at 7:1 prepolymer:crosslinker ratio) was poured onto the master to fill the support. Room temperature curing is critical to prevent deformation of the flatness of the molded surface from heat shrinkage. The layer is left to cure for 48 hours at room temperature on a level surface. After curing, the device is carefully removed from the mold by prying it free with a straight edge razor blade and lubrication with 70% ethanol and 30% water solution. Inlets and outlets are cored into the embedded PDMS using a 0.75 mm-diameter biopsy punch (Z708798, Sigma-Aldrich, St. Louis, MO). 70% ethanol solution is injected into the inlets and outlets to rinse away any remaining PDMS debris.

Exclusion molding of thin PDMS layers

The thin PDMS layer was produced with 400 μm tall vias and 200 μm tall microchannel features using exclusion-molding technique (see Fig. S2). The master mold was placed on four sheets of polyester film on a 4″ diameter, 0.5″ thick steel disc. Uncured PDMS (7:1) was mixed, degassed, then poured onto the master, and degassed again to remove any residual air bubbles from the features. A sheet of polyester film was placed onto the uncured PDMS taking care to prevent trapping of air. Using a straight edge razor blade, the surface of the film was smoothened against the SU-8 features of the master. Next, four additional sheets of polyester film and a 4″ diameter, 1/8″ thick acrylic disc were stacked on top of the mold to add compliance to the stack. Finally, another steel disc was placed on top and the assembly was compressed using a no-twist C-clamp (#5046A18, McMaster-Carr, Santa Fe Springs, CA). The mold was allowed to cure overnight at room temperature before baking for 1 hour in a convection oven at 70 °C. Room temperature curing was used because PDMS cured at elevated temperatures shrinks after cooling causing problems with registration of layers. Upon disassembly of the molding apparatus, the PDMS layers were cut out from the master using a sharp blade and placed onto a clean sheet of polyester film in preparation for plasma bonding. Care must be taken to ensure air bubbles and dust do not deform the flatness of the PDMS layer when applied to the film, so this step was done in a clean room.

Plasma bonding assembly and silane coupling of membranes

Transparent PET track-etched membranes with 1.0 μm pore size and a porosity of 1.6×10^{10} pores/m^2 (BD Bioscience, #353102) were activated with oxygen plasma using 60 W, 670 mtorr, 60 sec, and 40 kHz RF from a Zepto plasma system (Diener Electronic GmBH, Ebhausen, Germany). After plasma oxidation membranes were then submerged in a silane mixture of 2% bis-amino silane, 1% water, and 97% isopropanol or 20 min at 80 °C on a hotplate. After treatment, the silane modified membranes were rinsed with copious isopropanol, cured for 30 min in a convection oven at 70 °C, then soaked in 70% ethanol in water solution for 30 min while the PDMS layers of the device were assembled. The PDMS layers were assembled using oxygen plasma to bond the exclusion and embedded layers (shown in Fig. 2(B–C)). After curing for 5 min at 80 °C, the devices were allowed to cool then activated with oxygen plasma again and bonded to the silane modified membranes while wetted with a small amount of 70% ethanol in water solution to facilitate positioning and smooth contact with the PDMS. The surface of the membranes were dried using a compressed N_2 air gun, and then the devices were placed in a convection oven to cure at 70

Author Manuscript Author Manuscript Author Manuscript Author Manuscript

°C. After curing, the excess membrane around the perimeter of the PDMS was removed using dissection tweezers to complete the devices.

Finite-element modeling

The finite-element software COMSOL Multiphysics was used to generate 3D models of the microfluidic transwell insert. Simulations were computed on a MacBook Pro with a 2.3 GHz Intel Core i5 processor, 16 GB RAM, and a solid-state drive. The Free and Porous Media Flow physics module was used to simultaneously solve for the free flow in both the microchannels and 6-well, and porous flow in the track-etched membrane for the microfluidic transwell devices. The Free and Porous Media Flow module approximates the physics at the interface between the free flow and porous regimes using the Navier-Stokes and Brinkman equations in a single domain model. The simulated area includes the device microchannel network, membrane, and the 20 mm diameter-external fluid space of the 6-well plate as depicted in Fig. S3.

Operation of devices

For standard operation, microfluidic transwell devices were first treated with oxygen plasma for 1 min using the same conditions for bonding. Immediately after plasma activation, devices were flushed with a few mL of water using a syringe and blunt 22g dispensing needle to connect to the inlets and outlets. For cell culture, devices were then immersed in water in a 6-well plate and UV-sterilized for at least 2 hours. Flow and solutions were supplied to the devices using a Fusion Touch 100 syringe pump (Chemyx Inc., Stafford, TX) and 3 mL syringes with luer lock fittings, blunt dispensing needles, and thin bore Tygon tubing (Cole Parmer, Vernon Hills, IL).

Microscopy

Images were collected using a Nikon Eclipse Ti model inverted microscope equipped with automated objectives, fluorescence filter turrets, translational stage, and z-positioner (Nikon Instruments, Melville, NY). Images were acquired with a 12-bit cooled CCD camera (ORCA-ER, Hamamatsu, Japan). Nikon Elements-AR software was used to control acquisition and devices. A Perfect Focus System (PFS) module enables rapid, automated focusing through the detection of the cover glass interface of 6-well plates. Large surface area (20 mm diameter), phase-contrast and fluorescence images were stitched together in large arrays of overlapping fields of view. An important feature, the PFS enables rapid acquisition of a large number of images in combination with the translational stage to generate high-quality time-lapse image sets. For on-stage incubation and imaging of cells, we used a Live-Cell stage insert (Pathology Devices, USA) that allows for CO_2 and temperature control.

HL-60 cell culture and chemotaxis assay

We used the promyelocytic leukemia HL-60 cell line which can be differentiated to a neutrophil-like phenotype using protocols adapted from Collins[52] and Hauert et al.[53]. HL-60s were obtained from American Type Culture Collection (Manassas, VA). Cells were grown and sub-cultured using RPMI 1640 with L-glutamine, 25 mM HEPES, and phenol

Author Manuscript Author Manuscript Author Manuscript Author Manuscript

red which was supplemented with 10% heat-inactivated fetal bovine serum and 1% antibiotic-antimycotic. Cells were propagated at initial concentrations of $0.1–0.2\times10^6$ cells/mL and passaged every 3–4 days before they reached 1×10^6 cell/mL. For differentiation, cells were passaged into fresh medium with 1.3% dimethyl sulfoxide at $0.1–0.2\times10^6$ cells/mL for 4–7 days during which cells adopt a granular and irregular morphology. Gey's medium was used for chemotaxis assays. Glass-bottom 6-well plates were treated with 1 μg/mL human fibronectin (FC010, Millipore, Billerica, MA) for 15 min at room temperature. Wells were rinsed once with PBS solution then blocked for 15 min with 1% endotoxin-free BSA (Rockland Immunochemicals, Gilbertsville, PA). Neglecting the blocking step with the 1% BSA solution or using higher concentrations of fibronectin resulted in adherent cells that could not sufficiently detach in order to migrate. After blocking, the solution was aspirated and 200 μL of 20 nM fMLP in Gey's medium (F3506, Sigma-Aldrich, St. Louis, MO) was added to the well. 200 μL of cell suspension was dispensed into the well with the fMLP solution and allowed 15 min for cells to activate and attach to the surface. After attachment, the well was rinsed with 3–4 mL of fresh Gey's medium by gently rocking the plate and using gentle aspiration. The remaining cells were covered with 2 mL of 0.2% BSA in Gey's medium before applying the microfluidic transwell insert. The BSA facilitates cell motility by competing with the attachment of the cells to the coated surface. Devices were operated as described earlier by loading syringes with 0.2% BSA in Gey's medium and driving flow through tubing by a syringe pump. For the gradient source syringe, 100 nM fMLP was used with 1 μg/mL of 3 kDa Dextran-FITC for a fluorescent tracer to monitor the gradient. Typically, during preparation of substrates, the devices were setup and characterized using epi-fluorescence in a spare well plate. When cells were ready, the devices were transported to the cell culture hood and applied to the HL-60s in the sterile environment.

Image processing and tracking of HL-60 migration

The clear optical properties of the PDMS and PET materials used in the device allow for phase-contrast microscopy and large-area imaging of individual cells (see Fig. S4). Image processing and automated tracking of cell migration was accomplished in the FIJI package of Image J. The processed images (see Fig. S5) were assembled as a stack of tiffs and analyzed using the TrackMate plugin developed for Image J based on the algorithm described in Jaqaman et al.[54]. The algorithm uses a mathematical framework referred to as the Linear Assignment Problem (LAP) to achieve tracking of individual motile cells. TrackMate first identifies spots in each image of the stack given an estimated diameter of the cells (20 μm) and a threshold value for the minimum intensity. The Otsu method was applied using the built-in plugin to determine the optimal value for the threshold fed into TrackMate. For a full large-area stitched image it took approximately 10 min for spot detection in a stack of 200 images. Next, the plugin solves the LAP by linking spots between frames. We used a frame-to-frame max linking distance of 20 μm, and a gap-closing distance of 50 μm for a maximum duration of 5 frames. Gap-closing enables linking spots between frames when the cell drops out of detection for a few frames. Spurious debris or floating cells were manually removed from the tracks using the plugin. Epi-fluorescence was collected simultaneously to monitor the development of the gradient using a 3 kDa dextran-FITC as a tracer dye (Fig. S6).

Author Manuscript Author Manuscript Author Manuscript Author Manuscript

Retinal explant culture

Retinal explants were harvested from timed pregnant mice supplied by Charles River Laboratories. Pregnant mice were dissected in accordance with a protocol approved by the University of Washington Animal Care and Use Committee. The eyes of the E15 pups were enucleated while immersed in artificial cerebral spinal fluid bubbled with 5% CO_2 and 95% O_2. The retinal pigment epithelium, the lens, and the vitreous humor were extracted to reveal the intact retina tissue. Retinas were fragmented into quadrants and plated onto glass-bottom 6-wells that were coated with 25 μg/ml poly-d-lysine and 12.5 μg/ml laminin overnight at 4 °C. Medium used for retinal culture (Neurobasal, 2% B27, 1% N2, 2 mM GlutaMAX, 1% antibiotic-antimycotic) was supplemented with 0.4% methylcellulose. Methylcellulose increases the viscosity of the medium and assists in maintaining attachment of the explants. For normal cultures shown in Fig. S7, the addition growth factors, 50 ng/mL brain-derived neurotrophic factor (BDNF) and 10 ng/mL cilliary neurotrophic factor (CNTF), were added to medium as described by Barres et al.[55] For application of microfluidic transwell gradients, the retina explant was cultured for 3 days in the absence of growth factors.

Results and discussion

FEM simulations of microfluidic transwell gradients

The results in Fig. 3(A) describe the velocity field at a distance of 5 μm from the cell culture surface. Importantly, the flow velocities near the cell culture surface are low (~0–7 μm/min) in comparison to the delivery microchannel (~0–8.5×10^2 μm/min). Characteristically, the flow decelerates as it moves further from the delivery channels into the larger space of the well. The center of the device forms a stagnation point due to the opposing flows. The delivery channel is designed to have significantly lower flow resistance than the outlet and the membrane; therefore, the flow emerging from the membrane is uniform along the length of the delivery channel.

The concentration gradient generated at distance of 5 μm above the surface is shown in Fig. 3(B). Cross-sectional plots of the velocity and concentration profiles in the y–z plane are shown in Fig. 3(C–D). The flow emerging from the membrane impinges on the surface creating a pseudo-stagnation point, while the majority of flow curls away from the center of the device to the edge of the external fluid space. Notably, the concentration is uniform in the z-direction between the membrane and cell culture surface. The concentration profiles in Fig. 3(E) show gradients generated for a range of diffusing species from fluorescein to BSA at the same flow rate.

For cell culture studies, it is important to consider the effects of fluid shear stress on cell migration and cell viability. The shear stress imparted at the surface of the microfluidic transwell is described by the equation: $\tau = \mu\, \partial u/\partial z$, where μ is the dynamic viscosity, and $\partial u/\partial z$ is the change in the horizontal component of the velocity vector with respect to the z-axis. Due to the dominant viscous forces at low Reynolds numbers and the no-slip condition the velocity changes sharply near the walls of the microchannels. The effect of different flow rates on the chemotactic migration of neutrophils was reported by Walker et al.[36] They reported a migration bias along with the direction of flow for neutrophils in the presence of a

Author Manuscript Author Manuscript Author Manuscript Author Manuscript

shear stress greater than 687 mPa. For the laminar flow gradient device used in their analysis, the flow rates required to generate shear stress below this threshold limited the overall gradient size and the amount of space in which to analyze responsive cells[36,32]. For neurons the shear stress sensitivity is much higher; Wu et al.[56] used optically actuated particles to create rotational fluid shear stress adjacent to the growth cones of axons in culture and found that as little as 1.2 mPa was required to elicit turning in the direction of shear stress. Furthermore, Wang et al[57] found that fluid shear stress of only 7.2 mPa was enough to cause retraction of axon outgrowth. Low fluid shear stress is essential then not only for unbiased chemotaxis results, but also studies with sensitive cell types such as neurons. We simulated the shear stress at the surface for the microfluidic transwell using the results of the flow velocity predicted for 50 μL/hr as shown in Fig. 3(F). We found the shear stress at the cell culture surface to reach a maximum at 4.4×10^{-5} Pa, which is 4–5 orders of magnitude lower than the threshold for neutrophil migration bias and 2–3 orders of magnitude lower than the shear stress to induce growth cone turning.

Surface-fluorescence characterization of gradients

Surface-level gradients were quantified using an imaging technique for adapting regular epi-fluorescence microscopy to collect surface-level intensity[58]. We can limit the penetration length of the excitation light into our sample by flowing a mixture of non-fluorescent and fluorescent dyes, Orange G and fluorescein, respectively. The dyes are chosen because Orange-G absorbs strongly at the excitation wavelength (490 nm) and weakly at the emission wavelength of fluorescein (540 nm). In combination, the dyes compete for a finite amount of excitation energy. With an Orange G concentration of 40 mM, the characteristic penetration length is approximately ~4.9 μm (for which the excitation light intensity is 1/e times the incident intensity of the excitation light)[42]. Since the intensity of the excitation light decays exponentially as it penetrates the solution, 95% of the collected emission light is from within ~15 μm of the surface of the well plate. Using this technique, we characterized the stability and uniformity of the device by imaging over a large area of approximately 25 mm square area as shown in Fig. 4(A–B). Devices demonstrated evolution of gradient profiles to steady state at around 1 hour and long-term stability (here shown at 19 hours after continuous imaging and driving flow of 50 μL/hr). A comparison of the fluorescence intensity profiles taken across the gradient for every 2 min during evolution of the gradient shows strong similarity between the results of the time-dependent FEM simulations (Fig. 4(C–D)). The modular design also allows for manual positioning and rotation of gradients as shown in Fig. S8.

Diffusible tracers for live-monitoring

The surface-level fluorescence technique was used as a general method for characterizing different device designs and operating parameters, however it is not suitable for live cell culture applications because the Orange G dye is cytotoxic at the concentrations used. A desirable feature of any gradient generator is the ability to monitor the state of the gradient with standard optical microscopy. Since the concentration is uniform in z-direction of the device (see Fig. 3(D)) and the delivery channels are at the edges of the gradient space, the fluorescence collected from the bulk fluid volume using regular epi-fluorescence is linearly related to the surface concentration in the gradient region. Therefore, regular epi-

Author Manuscript Author Manuscript Author Manuscript Author Manuscript

fluorescence microscopy was used with fluorescently conjugated tracers to observe the development and steady state profiles for gradients generated with diffusing species of different molecular weights as shown in Fig. S9. In our device, equilibration time is not significantly influenced by the molecular weight of the diffusing species (as is the case for flow-free microfluidic gradient devices). A Péclet number (Pé) analysis for molecules with diffusivity from fluorescein to BSA reveals that convection and diffusion both contribute to the transport with 0.27>Pé>2.36 for the gradient region. Therefore, non-trivial flow in the external fluid space reduces the gradient equilibration time for slow diffusing species while maintaining similar gradient shapes (Fig. 3(E)).

Microfluidic transwell gradients for HL-60 chemotaxis

Microfluidic devices have been used to study neutrophil chemotaxis[32,38,40,59], migration in confined spaces[60], and directional decision-making[61]. For clinical applications, microfluidic devices have enabled on-chip isolation, assaying, and patient diagnosis[62–66]. To validate the microfluidic transwell platform we sought to observe unbiased chemotaxis by tracking the migration of a large population of cells; HL-60s, a neutrophil precursor cell line, were chosen because they have been shown to respond quickly to gradients and have been well-studied with microfluidic devices[60,67,64,65]. We assayed a large number of HL-60 cells using phase-contrast and time-lapse microscopy for gradients of 100 nM fMLP and controls.

Using the TrackMate plugin, individual cells were tracked for large-area images as shown in Fig. 5(A–B). The Chemotaxis and Migration Tool (Ibidi GmbH, Germany) for Image J was used to generate plots of the cumulative traces for each cell assayed as shown in Fig. 5(C–D). Using the plugin tool, the full traces were filtered to remove cells that were not migratory by applying a threshold of at least 10 μm in total displacement. From a total of 282 cells observed in the gradient, 208 migrated in the direction of the higher concentration of fMLP or 74% of cells. In comparison, an even distribution was seen for uniform fMLP and no fMLP with 51% and 50% of cells moving in the same direction of the y-axis without the gradient. We applied the Rayleigh statistical test for a circular distribution of points and found a low p-value ($p < 0.001$) indicating an irregular distribution. Controls did not have significant p-values. We applied further statistical analysis of various chemotaxis parameters as described in Zengel et al.[22] for the measure of forward migration index (FMI), directedness, velocity, and total displacement of cells for each condition as shown in Fig. 6. The FMI is calculated from the ratio of the vector component of the final displacement for each axis divided by the total accumulated cell path. The directedness is calculated from the ratio of the vector displacement to the total accumulated cell path. An unpaired Student-t test was applied between each condition. The mean FMI, directionality, and total displacement for the 100 nM fMLP gradient group were statistically significant ($p < 0.0001$). The mean velocity of the gradient and uniform group were statistically significant ($p < 0.0001$) demonstrating that fMLP stimulates motility even in the absence of a gradient. The FMI, directionality, and total displacement were not statistically significant between the two controls indicating that cells exposed to uniform fMLP tended to meander even though there overall migration speed and accumulated distance was greater.

Author Manuscript Author Manuscript Author Manuscript Author Manuscript

Interfacing microfluidic transwell gradients with retinal explant cultures

In a preliminary study, we have demonstrated the application of the microfluidic transwell device to an E15 embryonic mouse retinal explant cultured using conventional methods. The explant was first cultured in a glass-bottom 6-well plate using standard culture protocol for 3 days in vitro. The device was then applied to generate a gradient of 50 ng/ml BDNF and 10 ng/ml CNTF for the duration of 12 h as shown in Fig. 7(A). Large-area stitched images where taken with a time lapse to observe the resulting neuronal outgrowth. Since the microfluidic transwell is modular by design, we tested the effect of disrupting the outgrowth by removing the device, agitating the surrounding medium, and applying a new gradient of 20 μM Sp-8-Br-cAMP (Santa Cruz Biotechnology, CA) for a duration of 12 h (Fig. 7(B)). Sp-8-Br-cAMP is a cell membrane-permeable cyclic adenosine monophosphate (cAMP) analog[68]. We chose the second messenger cAMP because it is a key mediator of growth cone responses to a number of extracellular guidance molecules and previously implicated in micropipette-based studies with single neurons[69,68]. The resulting outgrowth of the explant in this experiment is suggestive of a gradient response. Further studies would be required to demonstrate significance, however, we believe that the example shown here demonstrates the potential of the microfluidic transwell insert design for interfacing with tissue cultures.

Conclusions

The microfluidic transwell insert enables generating concentration gradients in a user-friendly and modular format that is compatible with conventional cell cultures. Finite-element modeling was used to predict porous membrane flows, resulting gradients, and low shear stress. The device was used to analyze the chemotaxis of a large number of cells using direct visualization and automated image analysis. The modular design and low shear stress enabled interfacing with sensitive neuronal tissue explants. We believe that the microfluidic transwell is amenable to translation and dissemination to non-microfluidic oriented laboratories because it interfaces simply with standard cell culture 6-well plates. Future development of the device could improve automation using microvalves/micropumps[70] and pipette-accessible, on-chip reservoirs, or integration with a custom 6-well plate lid. The contributions to the development of microfluidic technology and in vitro gradient assay technique described here will prove beneficial to further study of gradient sensing biology.

Supplementary Material

Refer to Web version on PubMed Central for supplementary material.

References

1. Weijer CJ. Collective cell migration in development. J Cell Sci. 2009; 122:3215–3223. [PubMed: 19726631]
2. Sallusto F. The role of chemokine receptors in primary, effector and memory immune response. Exp Dermatol. 2002; 11:476–478.
3. Jin T, Xu X, Hereld D. Chemotaxis, chemokine receptors and human disease. Cytokine. 2008; 44:1–8. [PubMed: 18722135]

Author Manuscript Author Manuscript Author Manuscript Author Manuscript

4. Wartlick O, Kicheva A, González-Gaitán M. Morphogen gradient formation. Cold Spring Harb Perspect Biol. 2009:1.
5. Zlotnik A, Yoshie O. Chemokines: a new classification review system and their role in immunity. Immunity. 2000; 12:121–127. [PubMed: 10714678]
6. Tessier-Lavigne M, Goodman CS. The molecular biology of axon guidance. Science. 1996; 274:1123–1133. [PubMed: 8895455]
7. Song H, Poo M. The cell biology of neuronal navigation. Nat Cell Biol. 2001; 3:E81–E88. [PubMed: 11231595]
8. Dickson BJ. Molecular mechanisms of axon guidance. Science. 2002; 298:1959–1964. [PubMed: 12471249]
9. Roussos ET, Condeelis JS, Patsialou A. Chemotaxis in cancer. Nat Rev Cancer. 2011; 11:573–587. [PubMed: 21779009]
10. Godessart N, Kunkel SL. Chemokines in autoimmune disease. Curr Opin Immunol. 2001; 13:670–675. [PubMed: 11677088]
11. Gerard C, Rollins BJ. Chemokines and disease. Nat Immunol. 2001; 2:108–115. [PubMed: 11175802]
12. Goodhill GJ, Baier H. Axon guidance: stretching gradients to the limit. Neural Comput. 1998; 10:521–527. [PubMed: 9527831]
13. Levchenko A, Iglesias PA. Models of eukaryotic gradient sensing: application to chemotaxis of amoebae and neutrophils. Biophys J. 2002; 82:50–63. [PubMed: 11751295]
14. Imitola J, Raddassi K, Park KI, Mueller FJ, Nieto M, Teng YD, Frenkel D, Li J, Sidman RL, Walsh CA, Snyder EY, Khoury SJ. Directed migration of neural stem cells to sites of cns injury by the stromal cell-derived factor 1α/cxc chemokine receptor 4 pathway. Proc Natl Acad Sci. 2004; 101:18117–18122. [PubMed: 15608062]
15. Passier R, van Laake LW, Mummery CL. Stem-cell-based therapy and lessons from the heart. Nature. 2008; 453:322–329. [PubMed: 18480813]
16. Lindvall O, Kokaia Z, Martinez-Serrano A. Stem cell therapy for human neurodegenerative disorders–how to make it work. Nat Med. 2004; 10:S42–S50. [PubMed: 15272269]
17. Robinton DA, Daley GQ. The promise of induced pluripotent stem cells in research and therapy. Nature. 2012; 481:295–305. [PubMed: 22258608]
18. Restifo NP, Dudley ME, Rosenberg SA. Adoptive immunotherapy for cancer: harnessing the t cell response. Nat Rev Immunol. 2012; 12:269–281. [PubMed: 22437939]
19. Boyden S. The chemotactic effect of mixtures of antibody and antigen on polymorphonuclear leucocytes. J Exp Med. 1962; 115:453. [PubMed: 13872176]
20. Ming G, Song H, Berninger B, Holt CE, Tessier-Lavigne M, Poo M. Camp-dependent growth cone guidance by netrin-1. Neuron. 1997; 19:1225–1235. [PubMed: 9427246]
21. Zigmond SH. Ability of polymorphonuclear leukocytes to orient in gradients of chemotactic factors. J Cell Biol. 1977; 75:606. [PubMed: 264125]
22. Zengel P, Nguyen-Hoang A, Schildhammer C, Zantl R, Kahl V, Horn E. M-slide chemotaxis: a new chamber for long-term chemotaxis studies. BMC Cell Biol. 2011; 12:21. [PubMed: 21592329]
23. Nelson RD, Quie PG, Simmons RL. Chemotaxis under agarose: a new and simple method for measuring chemotaxis and spontaneous migration of human polymorphonuclear leukocytes and monocytes. J Immunol. 1975; 115:1650. [PubMed: 1102606]
24. Chen H, He Z, Bagri A, Tessier-Lavigne M. Semaphorin-neuropilin interactions underlying sympathetic axon responses to class iii semaphorins. Neuron. 1998; 21:1283–1290. [PubMed: 9883722]
25. Keenan TM, Folch A. Biomolecular gradients in cell culture systems. Lab Chip. 2008; 8:34. [PubMed: 18094760]
26. Kim S, Kim HJ, Jeon NL. Biological applications of microfluidic gradient devices. Integr Biol. 2010; 2:584.
27. Wu J, Wu X, Lin F. Recent developments in microfluidics-based chemotaxis studies. Lab Chip. 2013; 13:2484–2499. [PubMed: 23712326]

Author Manuscript Author Manuscript Author Manuscript Author Manuscript

28. Dertinger SKW, Chiu DT, Jeon NL, Whitesides GM. Generation of gradients having complex shapes using microfluidic networks. Anal Chem. 2001; 73:1240–1246.
29. Irimia D, Geba DA, Toner M. Universal microfluidic gradient generator. Anal Chem. 2006; 78:3472–3477. [PubMed: 16689552]
30. Cooksey GA, Sip CG, Folch A. A multi-purpose microfluidic perfusion system with combinatorial choice of inputs, mixtures, gradient patterns, and flow rates. Lab Chip. 2009; 9:417. [PubMed: 19156291]
31. Sip CG, Bhattacharjee N, Folch A. A modular cell culture device for generating arrays of gradients using stacked microfluidic flows. Biomicrofluidics. 2011; 5:022210–9.
32. Jeon NL, Baskaran H, Dertinger SKW, Whitesides GM, Van de Water L, Toner M. Neutrophil chemotaxis in linear and complex gradients of interleukin-8 formed in a microfabricated device. Nat Biotechnol. 2002; 20:826–830. [PubMed: 12091913]
33. Lin F, Nguyen CMC, Wang SJ, Saadi W, Gross SP, Jeon NL. Neutrophil migration in opposing chemoattractant gradients using microfluidic chemotaxis devices. Ann Biomed Eng. 2005; 33:475–482. [PubMed: 15909653]
34. Chung BG, Flanagan LA, Rhee SW, Schwartz PH, Lee AP, Monuki ES, Jeon NL. Human neural stem cell growth and differentiation in a gradient-generating microfluidic device. Lab Chip. 2005; 5:401–6. [PubMed: 15791337]
35. Saadi W, Wang SJ, Lin F, Jeon NL. A parallel-gradient microfluidic chamber for quantitative analysis of breast cancer cell chemotaxis. Biomed Microdevices. 2006; 8:109–118. [PubMed: 16688570]
36. Walker GM, Sai J, Richmond A, Stremler M, Chung CY, Wikswo JP. Effects of flow and diffusion on chemotaxis studies in a microfabricated gradient generator. Lab Chip. 2005; 5:611–618. [PubMed: 15915253]
37. Diao J, Young L, Kim S, Fogarty EA, Heilman SM, Zhou P, Shuler ML, Wu M, DeLisa MP. A three-channel microfluidic device for generating static linear gradients and its application to the quantitative analysis of bacterial chemotaxis. Lab Chip. 2006; 6:381. [PubMed: 16511621]
38. Frevert CW, Boggy G, Keenan TM, Folch A. Measurement of cell migration in response to an evolving radial chemokine gradient triggered by a microvalve. Lab Chip. 2006; 6:849. [PubMed: 16804588]
39. Keenan TM, Hsu CH, Folch A. Microfluidic 'jets' for generating steady-state gradients of soluble molecules on open surfaces. Appl Phys Lett. 2006; 89:114103.
40. Saadi W, Rhee SW, Lin F, Vahidi B, Chung BG, Jeon NL. Generation of stable concentration gradients in 2d and 3d environments using a microfluidic ladder chamber. Biomed Microdevices. 2007; 9:627–635. [PubMed: 17530414]
41. Shamloo A, Ma N, Poo M, Sohn LL, Heilshorn SC. Endothelial cell polarization and chemotaxis in a microfluidic device. Lab Chip. 2008; 8:1292. [PubMed: 18651071]
42. Bhattacharjee N, Li N, Keenan TM, Folch A. A neuron-benign microfluidic gradient generator for studying the response of mammalian neurons towards axon guidance factors. Integr Biol. 2010; 2:669.
43. Abhyankar VV, Lokuta MA, Huttenlocher A, Beebe DJ. Characterization of a membrane-based gradient generator for use in cell-signaling studies. Lab Chip. 2006; 6:389. [PubMed: 16511622]
44. Kim T, Pinelis M, Maharbiz MM. Generating steep, shear-free gradients of small molecules for cell culture. Biomed Microdevices. 2008; 11:65–73. [PubMed: 18688724]
45. Cate DM, Sip CG, Folch A. A microfluidic platform for generation of sharp gradients in open-access culture. Biomicrofluidics. 2010; 4:044105.
46. Mosadegh B, Agarwal M, Tavana H, Bersano-Begey T, Torisawa Y, Morell M, Wyatt MJ, O'Shea KS, Barald KF, Takayama S. Uniform cell seeding and generation of overlapping gradient profiles in a multiplexed microchamber device with normally-closed valves. Lab Chip. 2010; 10:2959. [PubMed: 20835429]
47. VanDersarl JJ, Xu AM, Melosh NA. Rapid spatial and temporal controlled signal delivery over large cell culture areas. Lab Chip. 2011; 11:3057. [PubMed: 21805010]
48. Kawada J, Kimura H, Akutsu H, Sakai Y, Fujii T. Spatiotemporally controlled delivery of soluble factors for stem cell differentiation. Lab Chip. 2012; 12:4508–4515. [PubMed: 22968416]

Author Manuscript Author Manuscript Author Manuscript Author Manuscript

49. Morel M, Galas JC, Dahan M, Studer V. Concentration landscape generators for shear free dynamic chemical stimulation. Lab Chip. 2012; 12:1340. [PubMed: 22344388]
50. Kim C, Kreppenhofer K, Kashef J, Gradl D, Herrmann D, Schneider M, Ahrens R, Guber A, Wedlich D. Diffusion- and convection-based activation of wnt/β-catenin signaling in a gradient generating microfluidic chip. Lab Chip. 2012; 12:5186–5194. [PubMed: 23108330]
51. Folch A, Toner M. Microengineering of cellular interactions. Annu Rev Biomed Eng. 2000; 2:227–256. [PubMed: 11701512]
52. Collins SJ. The hl-60 promyelocytic leukemia cell line: proliferation, differentiation, and cellular oncogene expression. Blood. 1987; 70:1233–1244. [PubMed: 3311197]
53. Hauert AB, Martinelli S, Marone C, Niggli V. Differentiated hl-60 cells are a valid model system for the analysis of human neutrophil migration and chemotaxis. Int J Biochem Cell Biol. 2002; 34:838–854. [PubMed: 11950599]
54. Jaqaman K, Loerke D, Mettlen M, Kuwata H, Grinstein S, Schmid SL, Danuser G. Robust single particle tracking in live cell time-lapse sequences. Nat Methods. 2008; 5:695–702. [PubMed: 18641657]
55. Meyer-Franke A, Kaplan MR, Pfrieger FW, Barres BA. Characterization of the signaling interactions that promote the survival and growth of developing retinal ganglion cells in culture. Neuron. 1995; 15:805–819. [PubMed: 7576630]
56. Wu T, Nieminen TA, Mohanty S, Miotke J, Meyer RL, Rubinsztein-Dunlop H, Berns MW. A photon-driven micromotor can direct nerve fibre growth. Nat Photonics. 2012; 6:62–67.
57. Joanne Wang C, Li X, Lin B, Shim S, Ming G, Levchenko A. A microfluidics-based turning assay reveals complex growth cone responses to integrated gradients of substrate-bound ecm molecules and diffusible guidance cues. Lab Chip. 2008; 8:227. [PubMed: 18231660]
58. Bancaud A, Wagner G, Dorfman KD, Viovy JL. Measurement of the surface concentration for bioassay kinetics in microchannels. Anal Chem. 2005; 77:833–839. [PubMed: 15679351]
59. Kim D, Lokuta MA, Huttenlocher A, Beebe DJ. Selective and tunable gradient device for cell culture and chemotaxis study. Lab Chip. 2009; 9:1797. [PubMed: 19495465]
60. Irimia D, Charras G, Agrawal N, Mitchison T, Toner M. Polar stimulation and constrained cell migration in microfluidic channels. Lab Chip. 2007; 7:1783. [PubMed: 18030401]
61. Ambravaneswaran V, Wong IY, Aranyosi AJ, Toner M, Irimia D. Directional decisions during neutrophil chemotaxis inside bifurcating channels. Integr Biol. 2010; 2:639.
62. Butler KL, Ambravaneswaran V, Agrawal N, Bilodeau M, Toner M, Tompkins RG, Fagan S, Irimia D. Burn injury reduces neutrophil directional migration speed in microfluidic devices. PLoS ONE. 2010; 5:e11921. [PubMed: 20689600]
63. Agrawal N, Toner M, Irimia D. Neutrophil migration assay from a drop of blood. Lab Chip. 2008; 8:2054–2061. [PubMed: 19023468]
64. Berthier E, Surfus J, Verbsky J, Huttenlocher A, Beebe D. An arrayed high-content chemotaxis assay for patient diagnosis. Integr Biol. 2010; 2:630–638.
65. Cavnar PJ, Berthier E, Beebe DJ, Huttenlocher A. Hax1 regulates neutrophil adhesion and motility through rhoa. J Cell Biol. 2011; 193:465–473. [PubMed: 21518791]
66. Meyvantsson I, Vu E, Lamers C, Echeverria D, Worzella T, Echeverria V, Skoien A, Hayes S. Image-based analysis of primary human neutrophil chemotaxis in an automated direct-viewing assay. J Immunol Methods. 2011; 374:70–77. [PubMed: 21215269]
67. Kress H, Park JG, Mejean CO, Forster JD, Park J, Walse SS, Zhang Y, Wu D, Weiner OD, Fahmy TM, Dufresne ER. Cell stimulation with optically manipulated microsources. Nat Methods. 2009; 6:905–909. [PubMed: 19915561]
68. Murray AJ, Tucker SJ, Shewan DA. Camp-dependent axon guidance is distinctly regulated by epac and protein kinase a. J Neurosci. 2009; 29:15434–15444. [PubMed: 20007468]
69. Song H, Ming G, Poo M. Camp-induced switching in turning direction of nerve growth cones. Nature. 1997; 388:275–279. [PubMed: 9230436]
70. Au AK, Lai H, Utela BR, Folch A. Microvalves and micropumps for biomems. Micromachines. 2011; 2:179–220.

Author Manuscript Author Manuscript Author Manuscript Author Manuscript

71. Oh KW, Lee K, Ahn B, Furlani EP. Design of pressure-driven microfluidic networks using electric circuit analogy. Lab Chip. 2012; 12:515–545. [PubMed: 22179505]

Author Manuscript Author Manuscript Author Manuscript Author Manuscript

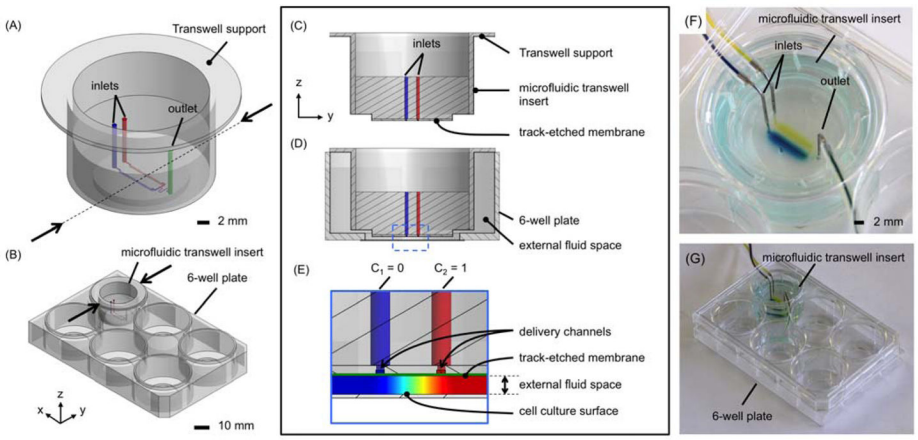

Fig. 1.

(A) A 3D rendering of the microfluidic transwell insert. The inlets supply flow to the embedded microfluidic channels (shown as red, blue, and green). (B) The device is designed for application to a glass-bottom 6-well plate. (C) A cross-sectional view of the device with the inlets shown. The bottom-most surface of the device and embedded microchannels is a track-etched membrane. (D) The device hangs self-supported in a 6-well. (E) A close-up view of the gradient region designated by the dotted blue box in (D) (not drawn to scale for clarity). The device defines an external fluid space between the track-etched membrane (green line) and the cell culture surface that is approximately 250 μm in height. The delivery channels provide flow through the membrane to generate a concentration gradient in the external fluid space (color map). (F–G) Photographs of a microfluidic transwell insert loaded with colored dyes. Yellow and blue dyes are used here to visualize the microfluidic network and gradient delivery to the external fluid space of the 6-well plate.

Author Manuscript Author Manuscript Author Manuscript Author Manuscript

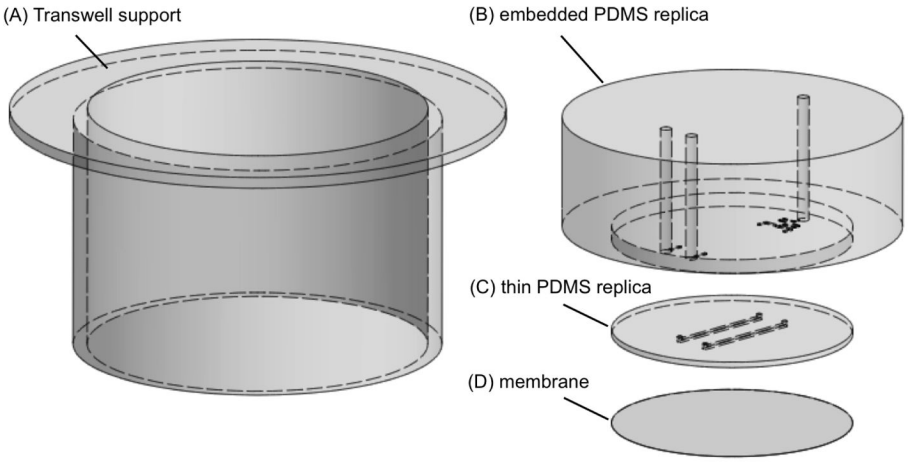

Fig. 2.

Multilayer soft-lithography and plasma bonding assembly of devices. (A) A transwell insert plastic support. (B) A microchannel featured PDMS replica is embedded in the plastic transwell support. (C) A thin PDMS layer is produced using exclusion molding technique. (d) A track-etched membrane is modified using a bis-amino silane method to render it reactive with oxygen plasma treated PDMS for hydrolytically stable bonding of the complete device.

Author Manuscript Author Manuscript Author Manuscript Author Manuscript

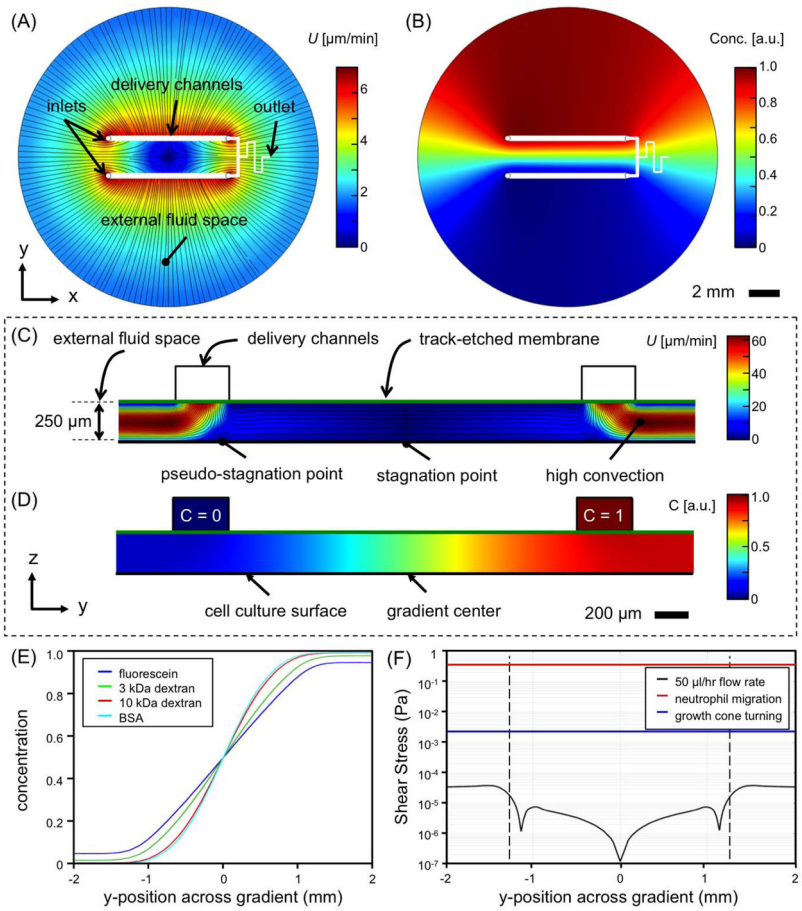

Fig. 3.

Results from the 3D FEM simulations of the microfluidic transwell. (A) The velocity profile at a distance of 5 μm above the cell culture surface using a flow rate of 50 μL/hr applied at the inlets. Streamlines designate the instantaneous direction of flow. Flow enters the 20 mm diameter and 250 μm thick external fluid space from the track-etched membrane along the length of the delivery channels or passes through the outlet. Opposing flow at the center of the device forms a stagnation point while the majority of flow escapes radially from the delivery channels. (B) The solution for the concentration gradient with fluorescein as the diffusing species ($D = 6.4\times10^{-10}$ m^2/s). Cross-sectional views show the (C) velocity profile and (D) the concentration gradient across the center of the device (at x = 0) in the y–z plane. The gradient is uniform in the z-direction. (E) A plot of concentration profiles across the cell culture surface in (C) for different diffusing species. (F) A log scale plot of the fluid shear stress with comparison to the shear stresses reported to induce neutrophil migration bias[36] and growth cone turning[56]. Local minima are the result of the central stagnation point and the flow impinging on the surface beneath the delivery channels (centers designated by dotted lines). The maximum shear stress exerted by the microfluidic transwell at 50 μL/hr is 4.4×10^{-5} Pa.

Author Manuscript Author Manuscript Author Manuscript Author Manuscript

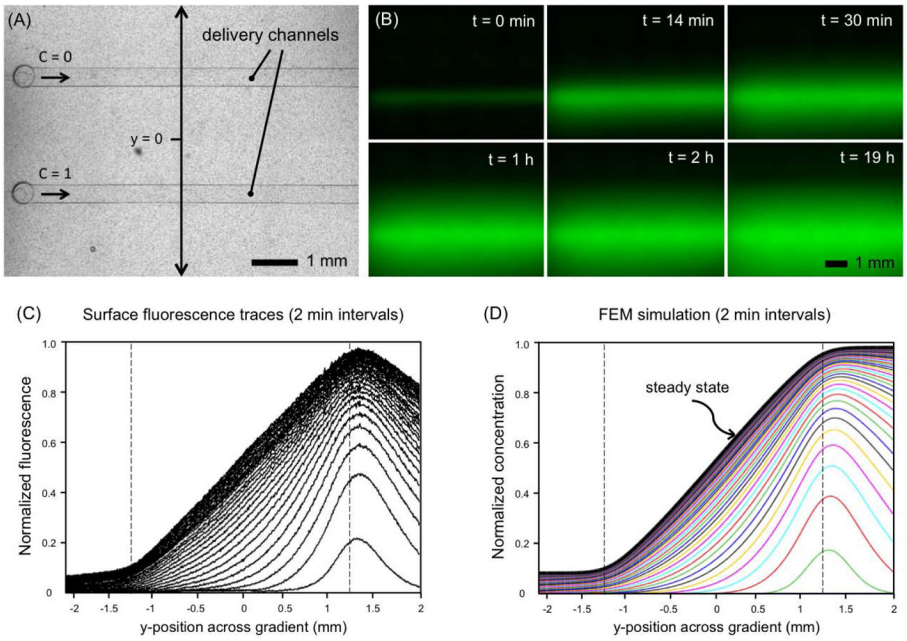

Fig. 4.

Characterization of the microfluidic transwell gradients using surface-fluorescence microscopy. (A) A large area bright-field image shows position of the device and features. (B) A time-series of surface-fluorescence images showing the evolution of the surface gradient with time for diffusing species ($D = 6.4\times10^{-10}$ m^2/s). At t = 0 min, the device was inserted into the well while flowing at a rate of 50 μL/hr. (C) Fluorescence intensity profiles were plotted along the y-axis in the position indicated in (A) for 19 hours in 2 min increments. (D) The FEM simulation predicts a similar behavior for the evolution of the gradient profile with time and steady state. Vertical dotted lines designate the center delivery channels with respect to the y-axis.

Author Manuscript Author Manuscript Author Manuscript Author Manuscript

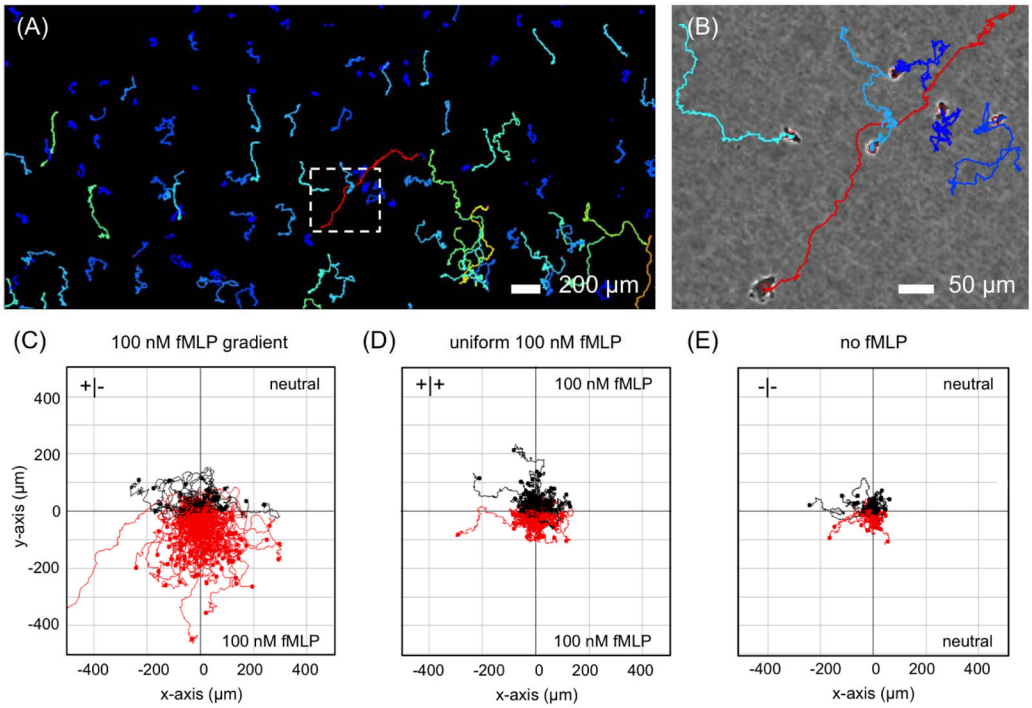

Fig. 5.

Tracking of HL-60 chemotaxis in microfluidic transwell gradients. (A) The TrackMate plugin results for a 100 nM fMLP gradient are shown for half of the tracked area. The color of the tracks represents increasing total displacement from blue to red in color. (B) Close-up view of the area in (A) showing the final frame of the original phase-contrast image and cell traces. Videos of the tracked image stacks shown in (A) and (B) are available online as supplemental information. TrackMate can resolve individual tracks for cells that migrate through crowded regions. Cumulative traces of cells for (C) gradient, (D) uniform, and (E) no fMLP. Red traces indicate cells that displaced in the direction of the negative y-axis.

Author Manuscript Author Manuscript Author Manuscript Author Manuscript

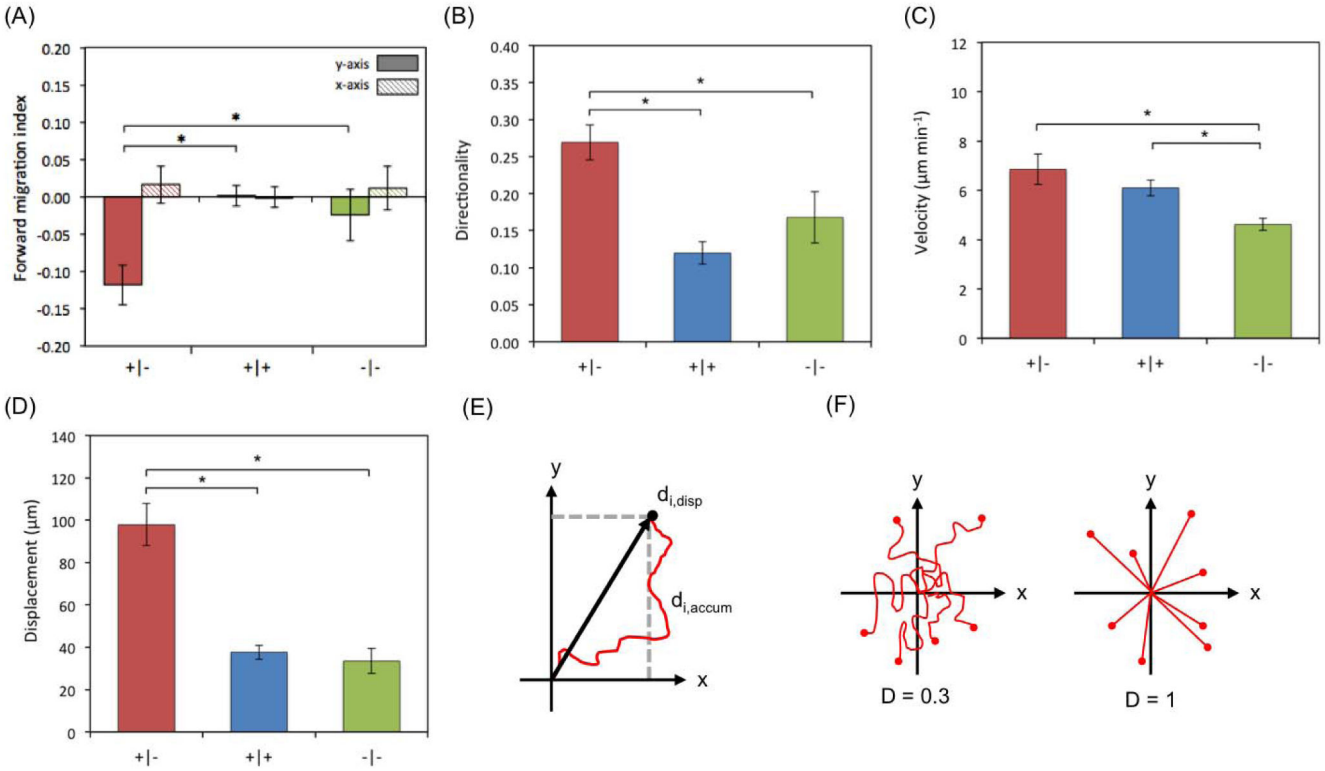

Fig. 6.

Analysis of HL-60 chemotaxis. Plots of the mean (A) forward migration index (y- and x-axis), (B) directionality, (C) velocity, and (D) displacement. Whiskers are 95% confidence intervals. (*) P-value < 0.001. (E) The forward migration index is the ratio of the displacement in the direction of either the x- or y-axis to the total accumulated distance. The displacement is the vector length of the final coordinates from the origin. (F) The directionality is a measure of the straightness of the cells trajectory (displacement/accumulated distance). Low directionality means cells follow a more meandering path.

Author Manuscript Author Manuscript Author Manuscript Author Manuscript

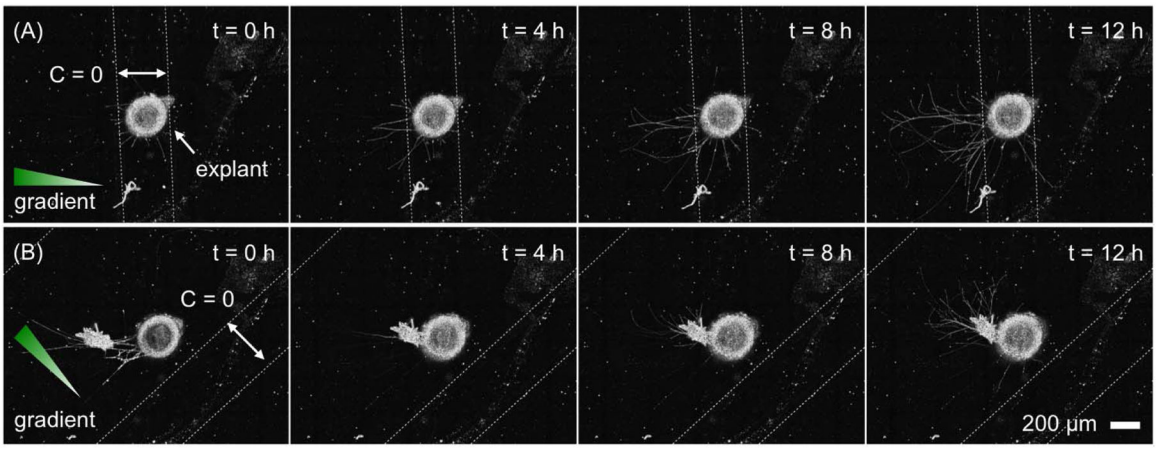

Fig. 7.

Application of growth factor and second messenger gradients to retinal explants. Images have been processed using edge detection with Image J to enhance the contrast of neurites against the background. The dotted white lines designate the edges of a delivery microchannel. (A) A retinal explant was cultured 3 days in vitro before application of the microfluidic transwell insert and generation of a gradient of 50 ng/ml BDNF and 10 ng/ml CNTF over the course of 12 hours. The delivery channel for C = 0 is positioned directly over the retinal explant with the gradient increasing to the left. (B) After removing the device and agitating the medium to cause retraction of the neurites, the device was replaced and a gradient of 20 μM sp-8-br-cAMPS at an angle of 45° was positioned across the explant. Time-lapse videos are available as supplemental files online.